Effect of sediment feed rate on bedload pulses in a gravel-bed flume

Blaise Dhont[1,*] **and Christophe Ancey**[1]

[1]École Polytechnique Fédérale de Lausanne, Lausanne, 1015, Switzerland
[*]corresponding author, blaise.dhont@epfl.ch

ABSTRACT

In engineered rivers, the disruption of sediment flux causes bed erosion and reduces the wealth of stream morphology. A large amount of work has been put into understanding how sediment shortage or supply impacts bed morphology and sediment transport. Earlier laboratory experiments showed that the bed response to sediment supply created considerable fluctuations of transport rates, making any quantification difficult. An obstacle to this quantification arises from the existence of various timescales characterizing the physical processes involved in the response. In this paper, we tackle this issue by studying how these timescales emerge from the analysis of bedload transport rates. We ran three experiments in a gravel-bed flume with the same water discharge, but with three different sediment feed rates. To explore the widest range of timescales, we acquired transport rates at high frequency over long durations. We also monitored bed evolution. The bed surface, initially flat, developed a row of bars and pools. Common sense (epitomized by Lane's balance) states that, at constant water discharge, a linear increase in sediment supply should lead to an equally linear increase in bed slope. We observed a more complicated behavior: the bed response admittedly experienced a (nonlinear) slope change, but more importantly a significant change of roughness caused by bedforms. Bedforms were not static, but evolved continuously giving rise to large fluctuations in the bedload transport rates in the form of bedload pulses. These bursts of activity were described through their mean duration, frequency of occurrence, and inter-arrival time. Bedload pulses were less frequent, larger, and lasted longer in experiments with lower feed rates. Our results suggest that sediment shortage strengthens the part played by bedload pulses in bedload transport: the bedload transport gets more intermittent while the bed plays a crucial buffer role between incoming and outgoing sediment.

Keywords: Sediment supply, Bedload pulses, Bed morphology, Flume experiment, River restoration

Introduction

Rivers worldwide have been increasingly engineered for protecting populations against floods and exploiting natural resources such as fertile lands, construction material, and hydropower (Wohl, 2018). The downside is that human development significantly affects sediment fluxes from production zones in upland valleys to deposition zones in deltas (Fryirs, 2013), disturbances that can jeopardize the protection of populations and ecosystems. Restoring river and sediment flux has become a decisive step in any effective and sustainable management of water streams. Indeed, sediment supply controls river morphodynamics to a large extent (Mueller and Pitlick, 2014; Elgueta-Astaburuaga et al., 2018). In supply-limited reaches, the bed responds to the imbalance between transport capacity and sediment transport through slope decrease and armor development (Madej et al., 2009). Interrupting sediment transport then causes rivers to incise their beds and erode their banks (Brandt, 2000; Battisacco et al., 2016). Reaches downstream of dams are an example in point. Furthermore, sediment shortage is generally accompanied by a decrease in morphological variability, which negatively impacts riverine ecosystems because of the loss of aquatic and riparian habitats, water quality, and fish spawning areas (Kondolf, 1997; Kantoush and Murasaki, 2010).

How stream morphology is changed by varying sediment flux has attracted much attention over the past decades. Channel adjustment to varying sediment inputs can be investigated in the field, as shown for instance by Lisle et al. (2000) and Zunka et al. (2015) for gravel-bed streams, but the surveys are challenging owing to the long response times of natural systems. In this respect, laboratory experiments seem all the more appealing that they make it possible to investigate a number of specific issues more carefully (Madej et al., 2009). Laboratory experiments have confirmed that in gravel-bed channels, reducing sediment supply causes a narrowing of the active transport corridor (Nelson et al., 2009), associated with bed degradation and coarsening. As observed by Venditti et al. (2012) in their flume experiments, the termination of sediment supply leads to the elimination of alternate bars and to a significant slope reduction accompanied by a decrease in mean bed shear stress. These experiments are consistent with our physical picture of bedload transport, but other experiments have revealed that its behavior is more complex. For instance, Podolak and Wilcock (2013) have documented how grain sorting, slope adjustment, and spatial variability of bed topography can contribute to adjusting the transport capacity to changes in sediment supply, while Francalanci et al. (2012) have shown that sediment transport capacity can be adjusted through local variability of bed shear stress without changing mean stress values.

Sediment replenishment has often been implemented in river restoration projects since the late 1980s to counter the negative effects of sediment flux disruption, especially the decrease in channel complexity (Battisacco et al., 2016). The efficiency of this strategy depends on the extent and sustainability of the morphological changes to the bed (Sklar et al., 2009). Optimizing sediment injection patterns has thus spurred research into how sediment pulses alter channel-bed morphology (Battisacco et al., 2016). The morphological response to sudden increases in sediment supply seems to depend on the initial bed topography. Zunka et al. (2015) have reported that pulses tend to smooth bed topography in gravel-bed channels with initially high relief, and inversely to roughen it when the initial relief variance is low. Sediment pulses have been reported to propagate primarily by dispersion (Cui et al., 2003), but pulse translation can be significant when the bed is armored (Sklar et al., 2009). When pulse amplitudes are high enough, the bed can aggrade and start to braid (Hoffman and Gabet, 2007).

Sediment pulses in gravel-bed rivers do not solely arise from human-driven injections or sudden natural inputs (such as landslides and debris flows): bedload transport in gravel-bed rivers is intermittent by nature. The earliest field measurements in the 1930s demonstrated that spatial and temporal variability is an inherent characteristic of bedload transport (Gomez, 1991). For decades, this variability had been downplayed or considered reflecting error measurements. With the progress made in the measurement techniques, doubts have been removed, and an increasing number of studies have highlighted the part played by sediment rate fluctations in the dynamics of bedload transport (Emmett, 1975; Reid et al., 1985; Whiting et al., 1988; Cudden and Hoey, 2003; Ancey et al., 2008; Radice, 2009; Roseberry et al., 2012; Furbish et al., 2016).

Bedload pulses can be defined—loosely for the moment—as bursts of particle activity featured by long and high fluctuations of the sediment transport rate, with peak values many times greater than the mean transport rate. They have been observed in flume experiments even under steady flow and sediment feed rate conditions in single thread (Kuhnle and Southard, 1988; Gomez et al., 1989; Recking et al., 2009; Dhont and Ancey, 2018) and braided channels (Ashmore, 1991; Hoey and Sutherland, 1991). Experiments were mostly performed with poorly-sorted sediment, but occasionally with well-sorted mixtures (Gomez et al., 1989; Dhont and Ancey, 2018), which shows that grain sorting is not the only mechanism involved. Large bedload pulses have long been considered to be caused by migrating bars (Miwa and Daido, 1995; Gomez et al., 1989) and low-relief bedforms such as sediment waves (Ashmore, 1991), bed waves (Hoey,

1992) and bedload sheets (Kuhnle and Southard, 1988; Recking et al., 2009). The terminology being not stable across the disciple, we have used the same definitions as James (2010), who clarified the concepts of sediment waves and related expressions. In the following, we call *sediment waves* low-height bedforms, whose migration is reflected by local changes in bed elevation.

Providing a more accurate definition of bedload pulses involves defining their characteristic times relative to other times featuring bedload transport. The question is simple, but not the answer. Bedload transport rate fluctuations occur over a wide range of timescales, some reflecting the movement of individual particles (Ancey et al., 2008, 2015; Heyman et al., 2013; Ma et al., 2014), others associated with global changes in river reach morphology (Hoey, 1992; Jerolmack and Paola, 2010). Surprisingly, whereas bedload transport rates vary randomly around mean values under steady state conditions, experiments have provided evidence for the periodic occurrence of pulses (Kuhnle and Southard, 1988; Gomez et al., 1989; Ashmore, 1991; Hoey, 1992; Ghilardi et al., 2014b). These periodic pulses were reported to result from the migration of macroscopic bedforms (that is, bedforms such as bars, whose dimensions scale with the channel width) over periods of time ranging from minutes to hours. One tentative explanation is that bedload transport combines both stochastic and deterministic processes, the stochastic component resulting from the intrinsic fluctuations of particle trajectories, and the deterministic part reflecting the motion of bedforms. Yet, taking a closer look at transport rates reveals that this decomposition into stochastic and deterministic components is not well supported by measurements when taking them at high frequency over very long periods (Dhont and Ancey, 2018).

Much of the earlier investigations have provided qualitative insights into how sudden variations in bedload flux impact stream morphology. Recently, some studies have started to quantify sediment transport rate variability as a result of varying sediment supply. Typical examples include the works of Saletti et al. (2015) and Elgueta-Astaburuaga et al. (2018), who imposed suddenly varying feed rates at their flume inlet, and then looked at how the characteristic times (defining the forcing of sediment supply) control the bedload transport rate at the flume outlet. Yet, a particular difficulty in this exercise is that little is known about the response time of the system (here, the flume) in the absence of forcing. If the system was linear, the natural timescales (i.e., the response time under steady feed rate) would appear spontaneously in the course of the analysis, but there is little hope that it is (Singh et al., 2009).

In this paper, we take a closer look at this issue by running experiments at constant feed rates over long periods of time, and by analyzing how sediment supply is mediated by the mean bed slope and bed topography (bars and pools in our experiments). Bed topography varies significantly over time, causing the bedload transport rate to fluctuate widely around its mean value imposed by the boundary conditions. We will see that a key feature of our experiments is that the system (made of the bed and carried sediment) does not fluctuate gently around an equilibrium state, but on the contrary, oscillates between phases of intense bedload transport and periods with no significant particle activity. The bursts of activity are called *bedload pulses*. Special emphasis will be given to the mechanisms of creation of bedload pulses and their characteristic times (recurrence time and duration). Capturing the temporal dynamics of bedload pulses requires very long experiment duration. A technical challenge is thus to acquire data (topography and bedload transport rate) with a high spatial and temporal resolution while running the experiment for hundreds of hours. This paper's first part is devoted to the experimental protocol. Further information can be found in Dhont (2017) and Dhont et al. (2017). The second part presents the experimental results, with a focus on the dynamics of bedload pulses and their interplay with bedforms.

Methods

Experimental setup and procedure

The experiments were carried out in a 17-m long (16-m usable) and 60-cm wide tilted flume with glass sidewalls. The bed was initially 31.5-cm thick and made of well-sorted natural gravel. The apparent density of the sediment mixture was 1490 kg m^{-3} and the characteristic diameters were $d_{30} = 5.2$ mm, $d_{50} = 6.0$ mm, and $d_{90} = 7.7$ mm. The mean diameter was 5.5 mm with a corresponding standard deviation of 1.2 mm. At the flume outlet, the mobile bed was retained by a perforated plate of which aperture was controlled by two valves in order to adjust the subsurface flow and limit boundary effects due to flow resurgence (the valve aperture was set only once, prior to the experimental campaign). The upstream part of the flume was obstructed by a porous box filled with gravel to reduce boundary effects due to the flow incoming from the tank located just upstream. During the experiments, the tank was filled at the desired rate by a pump connected the water recirculation system. The sediment feeding apparatus consisted of a hopper delivering sediment at the flume inlet by means of a conveyor belt. The sediment feed rate was controlled by adjusting the speed of a rotating cylinder with slots which obstructed the hopper outlet. The sediment delivered by the conveyor belt was subsequently fed into the flume through a pin board (Galton's board) that distributed the gravel in the cross-sectional direction following a Gaussian distribution centered in the middle of the flume. The sediment flushed out from the flume was collected in a heavy-duty bag having a storage capacity exceeding 500 kg. When the bag was filled, which took between 8 h and 24 h, the experiments were paused and the sediment collected was transferred to the hopper by using a bridge crane.

A series of preliminary runs were conducted in order to define the range of sediment feed rate Q_s, flow rate Q_w, and slope i for which bars developed in the bed. These trials were based on the criteria given in Yalin (1972, 1992) and the values tested depended on the range of flow rates the pump could deliver. It appeared that values in the order of $Q_s = 5$ g/s, $Q_w = 15$ l/s, and $i = 1.6\%$, respectively, allowed for the development of gravel bars in the bed.

We conducted three experiments with different steady sediment feed rates (2.5 g/s, 5.0 g/s and 7.5 g/s) and under the same steady flow conditions (15 l/s) in order to assess the effect of sediment supply on bedload transport and bed morphodynamics (see Table 1). We varied the feed rate instead of the flow rate because the system placed at the flume outlet (to counter the effect oh hyporheic flows) was adapted to a fixed water discharge. The experimental campaign was limited to three experiments because our motivation was to perform very long experiments (i.e., hundreds of hours) for capturing the longest timescales. At the beginning of each experiment, the bed was flattened out, and the flume slope was set close to the "equilibrium" bed slope estimated during the trial runs (equilibrium bed is used here in a loose sense to refer to beds that apparently remain stable for several tens of minutes). In this way, the bed thickness was uniform along the flume length during the experiments, and the disruptive effect of hyporheic flows were minimized. The average stream velocity was about 1 m/s while the flow depth was 3.5 ± 0.5 cm at the beginning of the three experiments. The corresponding flow conditions were turbulent and supercritical.

The hopper had a finite capacity and needed to be refilled with the sediment collected at the flume outlet. We made a pause on a regular basis to do so. Each experiment therefore consisted of a sequence of runs punctuated by the maintenance operations. During each pause, the sediment bag was weighted, and its value compared to the average bedload transport rate during the run so that we could detect potential problems. The run duration was set to 8 h, making it possible to conduct two two runs a day (one during daytime and the other overnight). The run duration was increased up to 24 h from respectively run 12 and run 20 in experiment 1 and 2 for saving time. A few runs were not altogether completed because of pump failures. During the runs, the bed and water elevations were measured every 10 min by scanning the bed with the moving cart while the bedload transport rate was recorded continuously at the flume outlet using impact plates (see next subsection). The acquisition of these different measurements was synchronized and fully automated. Measurements made during the first 9 minutes (necessary to reach the desired flow rate) and the last minute (during which the discharge was being dropped to zero) of each run were ignored.

Transport rate measurements

The bedload transport rate was measured at the flume outlet using six impact plates mounted in-line in the cross-sectional direction. Each device consisted of an accelerometer housed in a water-proof aluminium box and a perforated steel plate both fixed on an aluminium support plate. They were placed vertically 5 cm away the flume outlet so that the grains leaving the flume hit the perforated grid. Each device was insulated from the support frame by a rubber sheet in order to avoid vibration propagation. These sensors were originally developed in our laboratory by Mettra (2014).

The vibrations caused by grain impacts were recorded continuously during the experiments at a frequency of 10 kHz. The signal of each accelerometer was then postprocessed to compute the number of impulses (that is, the number of oscillations above a threshold amplitude value). Indeed, the latter is a robust proxy for the bedload transport rate (Rickenmann et al., 2014), and was found to be linearly correlated with the bedload transport rate in previous experiments (Dhont et al., 2017). Postprocessing consisted of the following steps: (1) smoothing the signal using a 1000 Hz low-pass filter, (2) detecting the impulses larger than 25 mV, and (3) computing the number of impulses over 1-min time steps. The average bedload transport rates over 1 min (denoted by Q_s) were finally computed for each experiment based on the calibration curves established for each accelerometer during the calibration campaign conducted prior to the experiments. For comparison purposes, the bedload transport rates were normalized with respect to the average value in each experiment ($Q_s^\star$). The measurement accuracy of the impact plates was assessed based on 164 runs, each lasting between 30 s and 5 min, during which sediment was collected and weighted. The bedload transport rates measured by the impact plates and the bedload transport rates computed based on the weighing were then compared: the standard deviation of the residuals was found to be about 30% and the mean value close to zero. The reliability of the impact plates was further assessed once the three experiments were completed by comparing the accelerometer data with the weight of the sediment collected during each run: for the total mass of sediment transported (approximately 100 kg), the relative deviation between the two values was found to be lower than 10%.

Water and bed elevation measurements

The water and bed elevation measurements relied on two sensors mounted on a moving cart, which scanned the bed over its entire length: a series of ultrasonic probes and a laser-sheet imaging system. Each scan lasted about 3 min and covered a 14 m$\times$60 cm area since the first and the last meter of the bed could not be measured because of technical limitations. They were conducted automatically every 10 min during the runs and the reference level for the elevation measurements was the bottom of the flume. An additional control scan was performed between each run when the bed was dry (better measurement accuracy).

The water elevation was measured using 8 ultrasonic probes fixed on a support plate on the moving cart and equally spaced in the cross-sectional direction. Given the distance between the probes and the bed surface, each sensor measured the underneath average water elevation over a circular area of about 9 cm in diameter. During the scans, the data from the ultrasonic probes were acquired with a frequency of 1000 Hz and were subsequently sampled at 50 Hz to obtain 8 longitudinal profiles having ~5 measuring points per centimeter. Each profile was then smoothed using a Gaussian filter and converted into centimeters based on the calibration curves computed prior to the experiments. The water elevation was finally interpolated over a 14 m×60 cm grid with a spatial resolution of respectively 5 cm and 1 cm in the longitudinal and in the cross-sectional direction. The calibration of each ultrasonic probes was performed by measuring the elevation of six wooden boards successively piled up on the bed surface in such a way that elevation values between 25 and 39 cm were considered. The measurement accuracy of the probes was subsequently assessed using a similar procedure, and it was found to be finer than 2 mm. Note that the measurement accuracy is likely to be coarser when measuring the water elevation because of increased noise in the signal.

The bed elevation was measured using a laser-sheet imaging technique consisting of a color camera taking top-view images of a green laser sheet projected on the bed surface (Figure 1). The laser was powerful enough (50 mW) for its projection on the bed, after passing through the water, to appear clearly in the images taken by the camera. This technique therefore did not required the discharge to be stopped during the experiments. The camera and the laser were both fixed on the moving cart in such a way that their positions were aligned with the middle of the flume and their orientations (in the horizontal plan) corresponded with the cross-sectional direction. The camera was pointing perpendicularly toward the bed surface and the laser sheet had a 28.1° angle to the vertical. These settings were chosen so that the laser projection appeared on every image taken during the experiments regardless the variations in bed topography (i.e., it was always in the field of view of the camera). The camera was set to take 6 frames-per-second which corresponded to roughly one image every two centimeter in the longitudinal direction (~900 images per scan). Each frame was then orthorectified (i.e., corrected for optical distortions from the sensor system) and post-treated using an image processing algorithm in order to compute the coordinates of the laser projection in the image. Based on these coordinates, the bed elevation along the cross-section corresponding to the laser projection was subsequently calculated using trigonometrical relationships detailed below. Given the geometry of setup, we find

$$\frac{x}{d} = \frac{z}{f} \quad \text{and} \quad \frac{x}{x_L} = \frac{z - z_L}{z_L}, \tag{1}$$

which implies that

$$z = \frac{f z_L x_L}{f x_L - d z_L} \quad \text{and} \quad x = \frac{d z_L x_L}{f x_L - d z_L}, \tag{2}$$

with x the horizontal distance between the laser projection and the camera, d the distance corresponding to x on the camera sensor, z the height between the camera and the bed surface, and f the focal length of the camera. The parameters x_L and z_L depict indirectly the angle of the laser and its position compared to the camera (Figure 1). Based on equation 2, the bed elevation was computed along the cross-section associated with each image since x and z were the only unknown variables. Indeed, f is a property of the camera, d depends on the coordinates of the laser projection in the image (computed previously) and on the sensor characteristics (size and resolution), and x_L and z_L were computed prior to the experiments based on the camera and laser positions. The elevation data associated with each image were then referenced with respect to the flume based on the camera position corresponding to each image along with the height between the camera and the flume bottom. The camera position was indeed recorded during the scans by using a proximity sensor counting the teeth of the cart rail. The bed elevation measurements were finally interpolated over the same 14 m×60 cm grid as the water elevation measurements for comparison purposes. In order to account for refraction effects, the following correction was applied to the bed topography measurements:

$$z_b = z_w - 1.4(z_w - z_{b,raw}), \tag{3}$$

with z_b the bed elevation from the flume bottom corrected for refraction effects, $z_{b,raw}$ the bed elevation prior to correction, and z_w the water elevation from the flume bottom computed using the ultrasonic probes. This correction was derived based on the Snell-Descartes law applied to an air-water interface. Note that $z_w - z_{b,raw}$ is an estimation of the flow depth and that the factor 1.4 matches approximatively to the ratio between the water and air refractive indexes (≈ 1.33). The invariant parameters in Equation 2 (i.e., x_L, z_L, and the camera elevation with respect to the flume bottom) were computed accurately prior to the experiments using the procedure described above in reverse (i.e., knowing z and x). For that purpose, we placed a board recovered with graph paper on the bed surface (under dry bed conditions) at a known elevation. By repeating the operation at a different elevation, we had enough parameters to compute the laser angle and to solve the equation system. The measurement accuracy under dry conditions finally assessed by measuring the height of the steps of a PVC staircase of known dimensions (15 mm step height) placed on the bed surface: it was found to be finer than 1 mm. In order to assess the measurement accuracy when water was flowing in the flume, we compared the bed topography measured at the end of each run under dry conditions and the same topography measured just before the discharge was stopped. The root mean squared error of these measurements was found to be about 0.5 cm, the bed elevation being roughly 30 cm thick with variations mostly between ±5 cm.

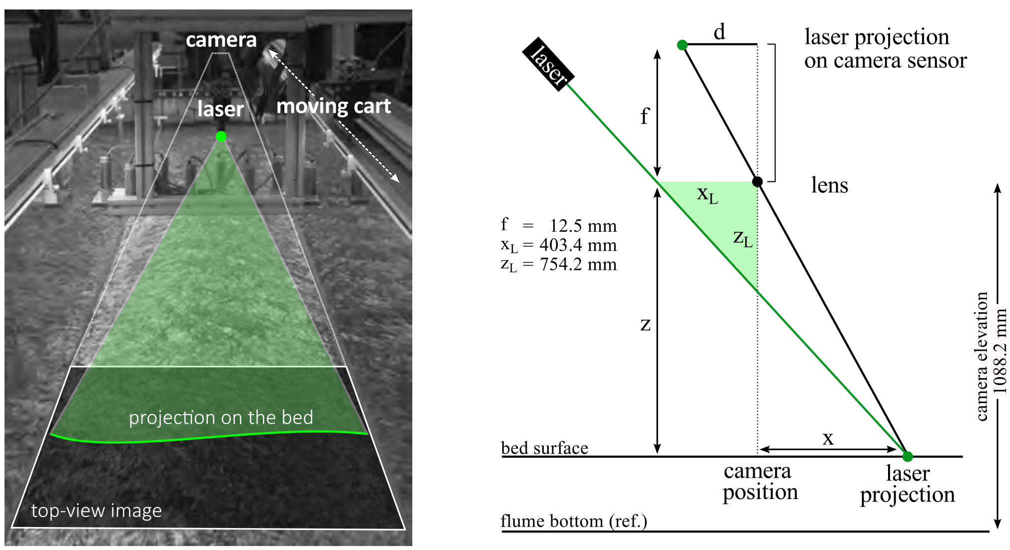

Figure 1. Front view (left) and schematic representation viewed from the side (right) of the laser-sheet imaging technique consisting of a camera and a laser mounted on a moving cart. Note that the schematic is not to scale and does not account for the refraction effects.

Results

Bed adjustment

The beginning of each experiment was characterized by an adjustment time (t_a) during which the bed evolved from the initial flat configuration to a formed morphology with bars and pools. This process started in the upstream part of the bed and propagated progressively in the downstream direction in the form of short migrating bars which grew in size. At the flume outlet, this transitional stage resulted in a period of very low sediment transport followed by intense pulses. During the adjustment time, the bed slope (S_b) first increased because of sediment deposition in the upstream part of the flume. After a certain breaking point, S_b dropped below its initial value as the bed was intensely eroded and sediment pulses recorded. At this point, bars had developed over the entire flume length and S_b finally came close to its average value over the entire experiment duration $\bar{S}_b$. In this study, the adjustment time was therefore defined as the time necessary for S_b to meet $\bar{S}_b$ for the first time. The topographical and sediment transport measurements recorded during this initial transitional stage of the experiments are ignored in the following. Note that the average bed slope is close to the flume slope in each experiment (Table 1), although slightly milder, which indicates that the average bed thickness remained about constant along the flume length during the experimental runs.

The bed topography in each experiment was characterized by single-row alternate bars consisting of a succession of bars and pools on either side of the flume (Figure 2). Bar heads (that is, the downstream limit and highest point of bars marking the transition toward the next pool) were most of the time in flush with the water surface, and deflected the flow toward the adjacent pools, as described by Lisle et al. (1993) and Lanzoni (2000). The depth of the pools was of the order of 10 cm, the flow velocity in the order of 1 m/s, and the flow regime close to critical with a Froude number varying about 1. The coordinate system of the topographical data is defined as follows: a longitudinal x-axis oriented in the upstream direction; a cross-sectional y-axis oriented from right to left with respect to the flow direction; and a vertical z-axis oriented upward (Figure 3).

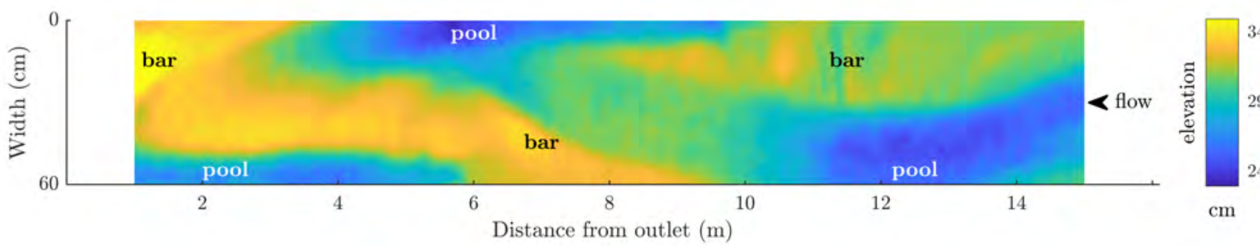

Figure 2. Typical bed topography observed during the experiments (example from E3). Three pools characterized by low bed elevations are visible: one on the right side and two on the left side of the bed.

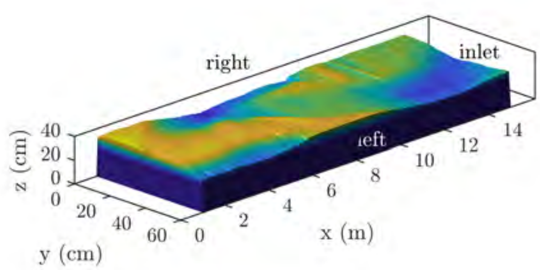

Figure 3. Coordinate system of the bed elevation data, the x-axis being the distance from the flume outlet, the y-axis the distance from the right wall of the flume, and the z-axis the elevation from the bottom of the flume.

The Shields number was computed in the same manner as in (Venditti et al., 2012) using the following equation:

$$\tau^{\star} = \frac{h_w \sin S_b}{(\rho_s - \rho) d_{50}}, \tag{4}$$

with h_w the water height, S_b the bed slope, ρ_s the sediment density, ρ the water density, and d_{50} the median grain diameter. The average Shields number during each experiment are given in Table 1. The average stream power is also given and was computed as follows:

$$\bar{\omega} = \rho g q \bar{S}_b, \tag{5}$$

with ρ the water density, g the acceleration due to gravity, q the unit water discharge, and $\bar{S}_b$ the average bed slope. The average dimensionless stream power index, given by $\bar{\omega}^\star = q\bar{S}_b/((\rho_{s,app}/\rho - 1)g{d_{50}}^3)^{0.5}$ with $\rho_{s,app}$ the sediment apparent density and d_{50} the median grain diameter (Hoey, 1992), was 0.36, 0.37, and 0.41, respectively, in experiment 1, 2, and 3.

The bed responded to increased sediment supply conditions by a general rise in the average bed slope, accompanied by an increase in the mean boundary shear stress and stream power, which resulted in an increased transport capacity (Iseya and Ikeda, 1987). This increase was more pronounced between experiment 3 and 2 than between experiment 2 and 1 although the sediment feed rate was augmented by the same amount. This nonlinearity in the bed slope response suggests that the adjustment mechanism is more complicated than what the common sense (epitomized by Lane's balance) says.

Table 1. Summary values related to the topographical measurements during experiment 1–3. The adjustment time t_a at the beginning of the experiments is ignored when computing the given statistics.

			E1	E2	E3
Flow rate	Q_l	l/s	15	15	15
Sediment feed rate	$Q_{s,in}$	g/s	2.5	5.0	7.5
Adjustment time	t_a	min	678	713	292
Effective experiment duration	T_{exp}	h	249.8	555.6	118.4
Flume slope		%	1.6	1.6	1.7
Average bed slope	$\bar{S}_b$	%	1.47	1.49	1.66
Standard deviation (absolute val.)		%	0.06	0.07	0.09
Average Shields number	$\bar{\tau}^\star$		0.08	0.08	0.09
Average stream power	$\bar{\omega}$	W/m^2	3.61	3.65	4.07

Transport rate fluctuations

Bedload transport rates were measured at the flume outlet during each experiment. The resulting time series exhibit large fluctuations (Figure 4) reflecting the alternation between low-transport phases and intense-transport events along the flume bed. The bedload transport rates could deviate from the average transport rate by one order of magnitude, and the coefficient of variation C_v (i.e., the ratio of the standard deviation to the mean) exceeded 100% in the three experiments (Table 2).

The peaks in the time series plotted in Figure 4 are called *bedload pulses* (Gomez et al., 1989). From a morphological perspective, the occurrence of such pulses implied that large amounts of sediment were transported in the downstream direction and that the bed was globally degraded because of sediment erosion. Between bedload pulses, the bedload transport rates were low compared to the sediment feed rates, which indicated an overall aggradation of the bed due to sediment deposition.

To study the characteristics of bedload pulses, we use the following operational definition: bedload pulses as any consecutive set of $Q_s^\star$ values above $\bar{Q}_s^\star$, the maximum of which is above a given threshold.

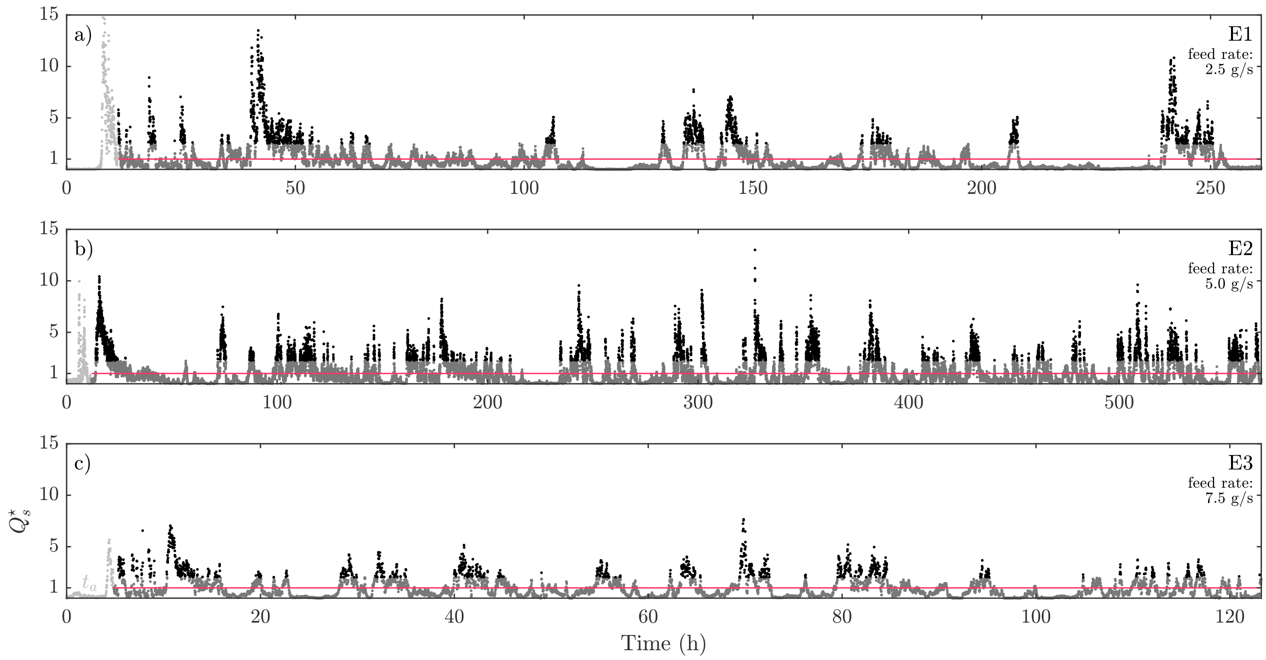

Figure 4. Time series of the normalized bedload transport rates ($Q_s^\star$) recorded during (a) experiment 1, (b) experiment 2, and (c) experiment 3. The solid lines indicate the normalized sediment feed rates ($Q_{s,in}^\star \approx 1$) and the transport rates larger than the mean value by at least one time the standard deviation are highlighted in black. The transport rates measured during the adjustment period (t_a) at the very beginning of the experiments are plotted in light grey.

Compared to the peak-over-threshold approach used in our earlier publication (Dhont and Ancey, 2018), this definition has the advantage of leaving the total number of pulses independent of the threshold value considered. However, it ignores that pulses associated with distinct timescales can overlap each other. The average pulse frequency and duration of bedload pulses exceeding the average value by more than the standard deviation (the pulses highlighted in Figure 4) are given in Table 2 for each experiment.

The coefficient of variation C_v and the average pulse frequency along with the corresponding standard deviation (Table 2) measure the intensity of the bedload transport rate fluctuations. This global characterization of the fluctuating behavior indicates that, in all three experiments, at least 30% of the bedload transport rate measurements are larger than two times the sediment feed rate. In addition, the pulses can be one order of magnitude higher or lower than the average transport rate. The intermittent character of the fluctuations is stressed by their relative high average frequency compared to the experiment duration and by the variability in the pulse period. Indeed, a bedload pulse is observed in average at least every five hours and the pulse spacing can vary within two orders of magnitude (from few minutes to more than ten hours). Note also that the average pulse duration is in the order of one hour, which is much lower than the average pulse spacing. These observations highlight the fluctuating behavior of all three bedload transport rate time series. However, comparing the characteristics of each experiment, they appear to be each associated with a different fluctuation regime depending on the sediment feed rate. Indeed, in experiments with larger sediment feed rates, bedload pulses tend to be shorter, more frequent, and of lower magnitude.

Bedload pulses are characterized by their duration, frequency, and magnitude. The statistics discussed above (Table 2) only regard pulses exceeding the standard deviation by one time. In the following, bedload

Table 2. Statistics of the bedload transport rates recorded during experiment 1–3. The adjustment time t_a at the very beginning of the experiments is ignored.

			E1	E2	E3
Experiment duration	T_{exp}	h	249.8	555.6	118.4
Sediment feed rate	$Q_{s,in}$	g/s	2.5	5.0	7.5
Average transport rate	$\bar{Q}_s$	g/s	2.57	4.84	7.97
Standard deviation		g/s	3.54	6.08	8.05
Normalized sediment feed rate	$Q^{\star}_{s,in}$		1.0	1.0	0.9
Normalized bedload transport rates					
Average value	$\bar{Q}^{\star}_s$		1	1	1
Range			0.00–13.50	0.00–13.00	0.00–7.66
Coefficient of variation	C_v		1.38	1.26	1.01
Statistics related to pulses larger than one time the standard deviation					
Average pulse frequency		h^{-1}	0.2	0.3	0.5
Average pulse period		h	5.2	3.5	2.1
Range			10 min–32 h	6 min–44 h	6 min–10 h
Standard deviation		h	7.0	5.3	2.2
Average pulse duration		h	1.2	0.9	0.6
Range			4 min–5 h	2 min–7 h	4 min–3 h
Standard deviation		h	1.3	1.0	0.6

pulses associated with each fluctuation regime are characterized by describing the dependency of their average frequency and average duration on their magnitude. For each experiment, the average pulse frequency and duration are computed by considering bedload pulses larger than different threshold values ranging from 1.5 to 4. The dependency of these three variables on each other is plotted in Figure 5. Threshold values larger than 4 are ignored because the number of corresponding pulses is too low for the related statistics to be significant.

The pulse frequency in Figure 5(a) decreases with increasing threshold value: low bedload pulses are more frequent than larger ones. In each experiment, this decrease can be described by a power law $f(x) = ax^b$ of which parameters are given in Table 3. In addition, bedload pulses are more frequent in experiments with larger sediment feed rates, irrespective of the threshold value considered. However, the average pulse frequency in each experiment converges toward zero with increasing pulse magnitude. In Figure 5(b), the average pulse duration increases linearly with increasing threshold value which indicates that in each experiment large bedload pulses tend to last longer than lower ones. The parameters of the linear regressions are given in Table 3. The slope of the regression lines is similar for experiment 2 and 3 whereas pulse duration increases about twice faster with pulse threshold in experiment 1 which had the lowest sediment feed rate. It appears also that the average pulse duration is longer in experiments with lower feed rates for any threshold value. The two relationships described above are combined in Figure 5(c) which shows that the average pulse frequency decreases with increasing average pulse duration. These relationships are similar in experiment 1 and 2 which have comparable average stream power values. In experiment 3, which has a larger average stream power, the average pulse frequency decreases faster

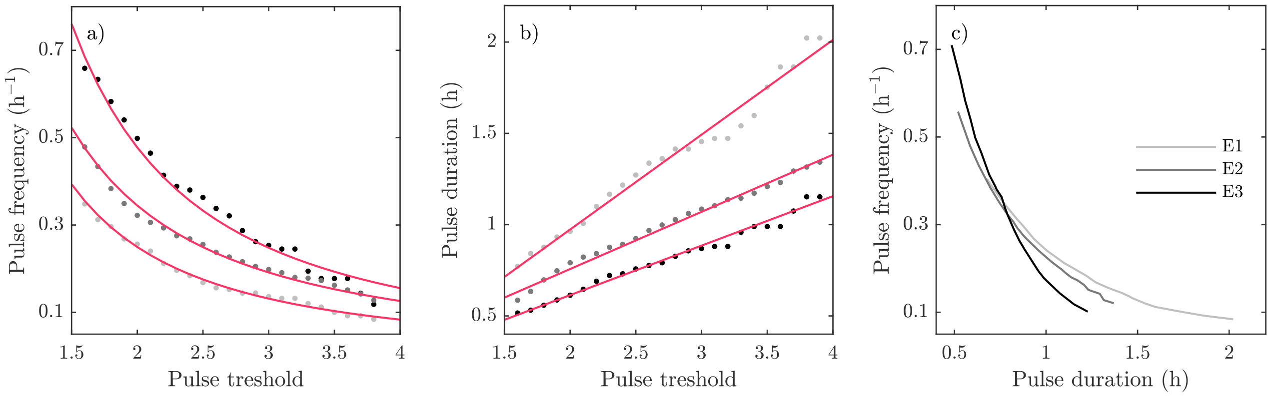

Figure 5. Dependency of pulse characteristics on the threshold used to define bedload pulses for experiment 1–3: (a) average pulse frequency versus pulse threshold, (b) average pulse duration versus pulse threshold, and (c) average pulse frequency versus the average pulse duration.

with increasing average pulse duration. Note that the range of values visited is however different in each experiment. These results therefore support the existence of three fluctuation regimes, each associated with a different sediment feed rate: bedload pulses tends to be shorter and more frequent, irrespective of the magnitude considered, when the feed rate increases.

As discussed above, the average pulse frequency and duration given in Table 2 depend on pulse magnitude (Figure 5). In order to complement the analysis on the intermittent character of bedload pulses, the relative standard deviation of the pulse duration and of the pulses inter-arrival times (i.e., their spacing over time) are plotted in Figure 6 as a function of the pulse threshold. The variability in pulse spacing in Figure 6(a) shows a minor dependence on pulse threshold although it exhibits a slight tendency to decrease. The average value of the relative standard deviation is respectively 1.4, 1.4, and 1.1 in experiment 1, 2, and 3 which is significant (i.e., it corresponds to coefficients of variation larger than 100%). This observation supports our previous conclusions that the bedload pulses observed are highly intermittent. The relative variability in pulse durations remains high (at least 60%) although the decrease observed with increasing threshold value in Figure 6(b) is steeper than that of pulse spacing. By comparing the average pulse duration in Figure 5(b) with the relative standard deviations in Figure 6(b), it appears that the pulse duration varies between few minutes and few hours which generalizes to any pulse threshold the above comment about the wide range of duration values observed (Table 2). The fluctuation regime in experiment 3 differs from the two others in Figure 6 by showing globally less variability in pulse duration and spacing: the intermittent character is less marked. In addition to highlight the intermittent character of bedload pulses, the high variability in pulse characteristics commented above implies that bedload transport rate fluctuations occur at different timescales.

Time scales of bedload pulses

For each experiment, the mean transport rate and sediment feed rate are very close (Table 2). This is usually interpreted as the telltale sign of bed equilibrium: what has gone out matches what has gone in over the experiment duration (Iseya and Ikeda, 1987). The question is how long it takes to observe a time-averaged transport rate that corresponds to the sediment feed rate.

This issue is addressed by computing for each experiment the *convergence time*, which is defined as the minimum sampling time for which the time-averaged bedload transport rate is sufficiently close to the sediment feed rate. As the time series exhibit large fluctuations, the convergence is slow. Here, "sufficiently

Table 3. Coefficients of the regression curves describing the dependency of the average pulse frequency and magnitude on pulse threshold for experiment 1–3. The goodness-of-fit is assessed based on the coefficient of determination R^2 and the standard error of the estimate SE.

	a	b	R^2	SE
	$f(x) = ax^b$, $x \in [1.5,4]$			
Experiment 1	0.75	-1.58	0.99	0.01
Experiment 2	0.94	-1.45	0.99	0.01
Experiment 3	1.47	-1.62	0.98	0.03
			see Figure 5(a)	
	$f(x) = ax + b$, $x \in [1.5,4]$			
Experiment 1	0.52	-0.06	0.98	0.06
Experiment 2	0.31	0.13	0.99	0.03
Experiment 3	0.27	-0.07	0.98	0.03
			see Figure 5(b)	

close" means that the time-averaged transport rate matches $Q_{s,in}$ to within 50%. The corresponding sampling time is denoted by $T_{c,50}$. Taking the time average of the normalized bedload transport rates for different sampling times T_s and starting times t_0 leads to:

$$\bar{Q}_s^\star(T_s;t_0) = \frac{1}{T_s} \sum_{t=t_0}^{t_0+T_s-1} Q_s^\star(t), \quad t_0 \in [1, T_{exp}] \quad \text{and} \quad T_s \in [1, T_{exp} - t_0 + 1], \tag{6}$$

with T_{exp} the experiment duration. The sampling times are chosen as multiples of 30 min and the starting times as multiples of 1 h in experiment 1 and 3. For convenience purposes, the starting times are multiples of 4 h in experiment 2, which is much longer than the two others. The adjustment time is ignored in each experiment.

The envelope of the time-averaged bedload transport rates computed for different t_0 values indicate the range of values visited by the bedload transport rates for different sampling times ranging from 1 min to 100 h (Figure 7). The upper envelopes therefore give the upper bound of bedload transport rates as a function of T_s, and reflect the effect of the sampling time on bedload pulses. The upper envelopes converge slowly to the sediment feed rates with increasing sampling time, and the convergence time to be longer in experiments with lower sediment feed rates. This result supports the previous observation that bedload pulses in fluctuation regimes related to larger sediment feed rates are lower in magnitude and closer in time.

The convergence times are long compared to the duration of the experiments (Table 4) even though the criterion chosen (e.g., pulses lower than $Q_{s,in} + 50\%$) is little restrictive. Furthermore, the time-averaged bedload transport rates converge very slowly to $Q_{s,in}$ as the sampling time increases (Figure 7). A neutral sediment balance can be achieved only for experiments much longer than the corresponding convergence time, for instance by one order of magnitude. Such a condition is only met in experiment 2 and 3 (Table 4).

The time-averaged bedload transport rates converge asymmetrically to the sediment feed rate (Figure 7). As shown just above, the convergence of the upper envelope shows the dependency of bedload pulses on the sampling time. By contrast, the convergence of the lower envelope reflects how the time-averaged bedload transport rates are affected by the occurrence of phases marked by low bedload transport. At short

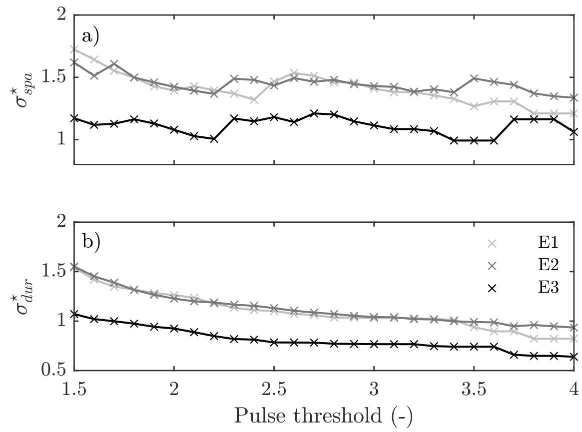

Figure 6. Relative standard deviation of (a) the pulse spacing σ^*_{spa} and (b) the pulse duration σ^*_{dur} as a function of the threshold value used to define bedload pulses in experiment 1–3.

Table 4. Convergence time related to the upper and lower envelope of the time-averaged bedload transport rates in experiment 1–3.

			E1	E2	E3
Sediment feed rate	$Q_{s,in}$	g/s	2.5	5.0	7.5
Experiment duration	T_{exp}	h	249.8	555.6	118.4
			criterion: $\max(Q_s) < Q_{s,in} - 50\%$		
Convergence time	$T_{c,50}$	h	64	38	13
$T_{exp}/T_{c,50}$			4	15	9
			criterion: $\min(Q_s) > Q_{s,in} - 50\%$		
Convergence time	$T_{c,50}$	h	84	46	18
$T_{exp}/T_{c,50}$			3	12	7

sampling times, the upper envelopes deviate from $Q^{\star}_{s,in}$ more significantly than the lower envelopes, which is consistent with the behavior of the time series in Figure 4: the difference between the bedload transport rates and $Q_{s,in}$ is much larger during bedload pulses than between them (i.e., during low transport phases). However, this tendency is reversed when sampling times are larger than respectively 57 h, 26 h, and 12 h in experiment 1, 2, and 3. The limiting factor for convergence then become the low transport phases. Note that this inversion occurs while bedload transport rate fluctuations are still significant (i.e., larger than $Q^{\star}_{s,in} \pm 50\%$). Consequently, the convergence times of the lower envelopes are longer than the ones related to bedload pulses (Figure 7). This slower convergence indicates that bedload pulses are generally of shorter duration than low transport phases. The above observations emphasize the importance of also considering low bedload transport phases when examining bedload transport rate fluctuations although, unlike bedload pulses, they are not responsible the massive transport of sediment. Indeed, the transport rates between bedload pulses can be much lower than the sediment feed rate during long time periods compared to the pulse duration. The large amounts of sediment stored in the bed during such low transport phases, and the morphological changes they necessarily imply, are likely to play a key role in the generation of bedload

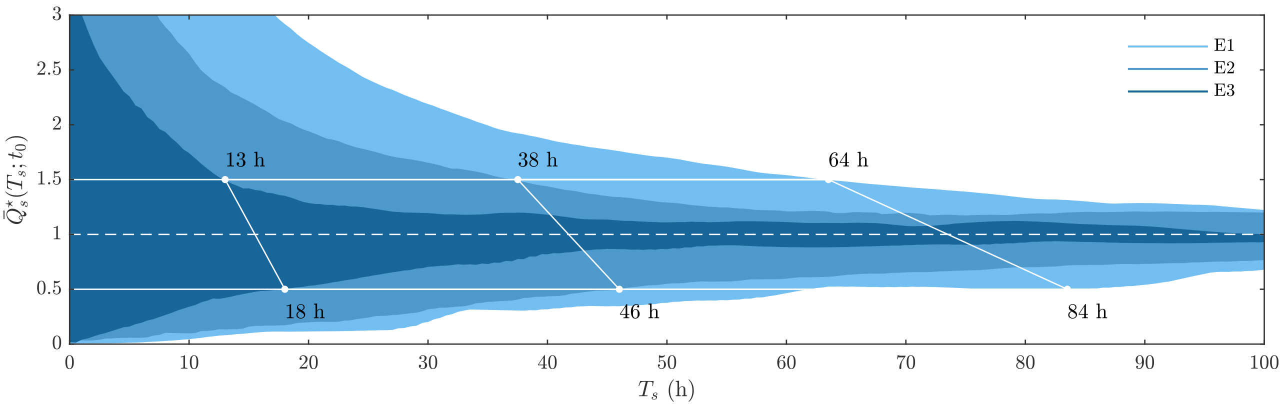

Figure 7. Envelopes of the normalized bedload transport rates as a function of the sampling time T_s for experiment 1–3. The dashed line indicates the normalized sediment feed rate ($Q^\star_{s,in}$) and the solid lines the convergence criterion ($Q^\star_{s,in}$ $\pm$ 50%).

pulses.

The slow convergence time of the time-averaged bedload transport rates indicates that the fluctuations recorded during the experiments occur over a wide range of timescales. The convergence time measures the time necessary to capture all types of autogenic fluctuations, including the largest ones. Hence, it can be interpreted as the upper bound of the fluctuation timescales. Indeed, bedload transport rate fluctuations are finite: they are bounded by the system size and the feeding conditions, as pointed out by Jerolmack and Paola (2010). The convergence time is therefore useful to evaluate the duration of the time series when investigating bedload transport rate fluctuations: the experiment should be longer than the convergence time by at least about one order of magnitude. Consequently, whereas experiment 2 and 3 seems long enough, experiment 1 is too short to capture the entire system dynamics. The observations made during experiment 1 should therefore be interpreted carefully.

The timescales of the bedload transport rate fluctuations range from a couple of minutes to more than ten hours. We therefore further investigate the time series in the frequency domain using the Thomson's multitaper power spectrum (Figure 8). The spectra saturate at low frequencies: the power spectral density is constant which is typical from white noise and reflects stationarity (Jerolmack and Paola, 2010). The characteristic timescale associated with saturation is about 33 h, 27 h and 13 h, respectively, in experiment 1, 2 and 3. They indicate the maximum timescale of bedload transport rate fluctuations and are consistent with the convergence times computed above. Moreover, the saturation timescale decreases with increasing sediment feed rate, which is consistent with our previous results. At frequencies higher than the saturation timescale, some frequencies are more energetic: they indicate the most prevalent periods of the fluctuations (Kuhnle and Southard, 1988). The power spectral density then decreases with increasing frequency. The log-log linearity observed at high frequency, from several hours to few minutes, indicates a scaling range reflecting a scale dependence of the fluctuation characteristics (Singh et al., 2009). The corresponding spectral slope is-1.62, -1.61, and -1.55 ,respectively, in experiment 1, 2 and 3. The energy contained in the fluctuations therefore decreases with increasing frequency similarly in each fluctuation regime, which suggests the occurrence of phenomena of the same nature.

We now examine the periodic behavior of bedload transport rate fluctuations for different timescales. A caveat is in order: *periodic* is used here to describe fluctuations that occur periodically. In some studies (Gomez, 1991; Hoey, 1992), *periodic* refers to any fluctuating behavior about a mean value. The autocorrelation function shows the correlation of a time series with itself taken at different time lags.

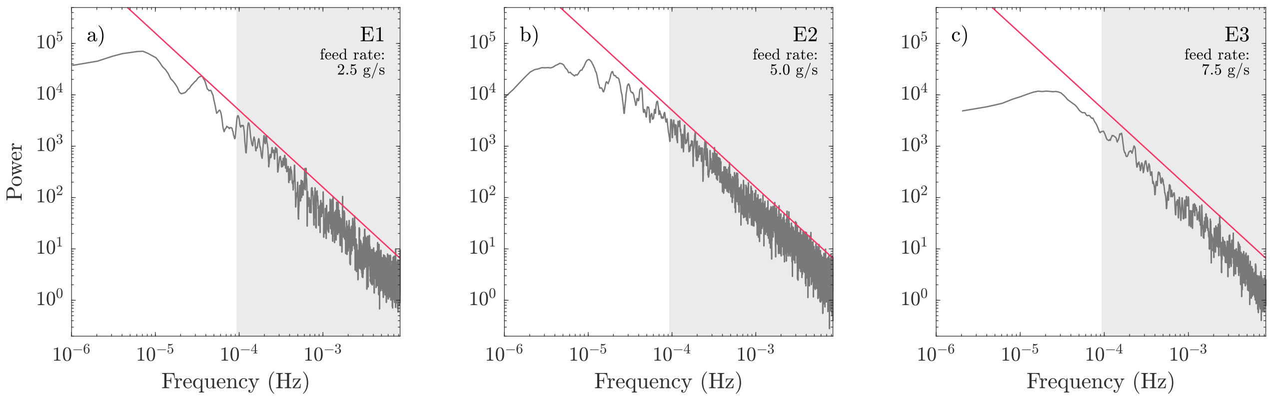

Figure 8. Power spectra of the bedload transport rates measured at the flume outlet during (a) experiment 1, (b) experiment 2, and (c) experiment 3. The scaling range is indicated in light grey and the -1.5 spectral slope is indicated.

We have computed it for each bedload transport rate time series (Figure 9). The effect of the sampling time is examined by computing the autocorrelation function for the bedload transport rates aggregated over different sampling times ranging from 1 h to 5 h. The autocorrelation functions get smoother with increasing sampling time, which is a direct effect of averaging. The general shape of the curves (including the peaks,) is, however, conserved even for sampling times as large as 5 h. The most prominent peaks therefore indicate the frequencies of bedload pulses associated with long timescales (i.e., several hours). The time lag when the autocorrelation function is zero for the first time represents the duration of large-scale pulses. It is 10 h, 8 h, and 3 h, respectively, in experiment 1, 2, and 3, which is in agreement with the pulse duration values given previously. This confirms that bedload pulses tend to be shorter when the sediment feed rate increases. In experiment 3, the autocorrelation function features several prominent peaks, which are evenly spaced by about 10 h. This regularity in peak spacing suggests that large-scale bedload pulses have a periodic behavior characterized by a period of about 10 h. This is consistent with the pulse frequencies obtained previously. In experiment 2, the most prominent peaks occur at time lags multiples of 26 h: large-scale pulses have a periodic behavior characterized by a period of about 26 h. Periodicity is thus less marked and of lower frequency for experiment 2 than for experiment 3 (which has a higher sediment feed rate). In experiment 1, a peak occurs at 6 h before the autocorrelation drops to zero. Some bedload pulses can therefore occur on regular basis with this period. The peak, however, vanishes for longer sampling times, which shows that periodic pulses are associated with timescales shorter than a couple of hours. The most prominent peak for experiment 1 occurs at a time lag of about 100 h, which is significant compared to the experiment duration (~260 h). Therefore, we cannot draw sound conclusions about periodicity for this experiment.

Morphological print of bedload transport

In order to examine the spatial distribution of bed degradation and aggradation processes, the average sediment erosion and deposition rates over the entire duration of the experiments were computed at each bed location. Erosion and deposition were found to offset one another everywhere in the bed. This balanced sediment budget indicates that the total mass of the bed is conserved at the experiment timescale and that intensely eroded zones also undergo substantial sediment deposition. The spatial distribution of the average deposition rates are plotted in Figure 10 for each experiment. Zones of intense deposition appear on both sides of the bed, alternatively near the right and left wall of the flume. They are stretched

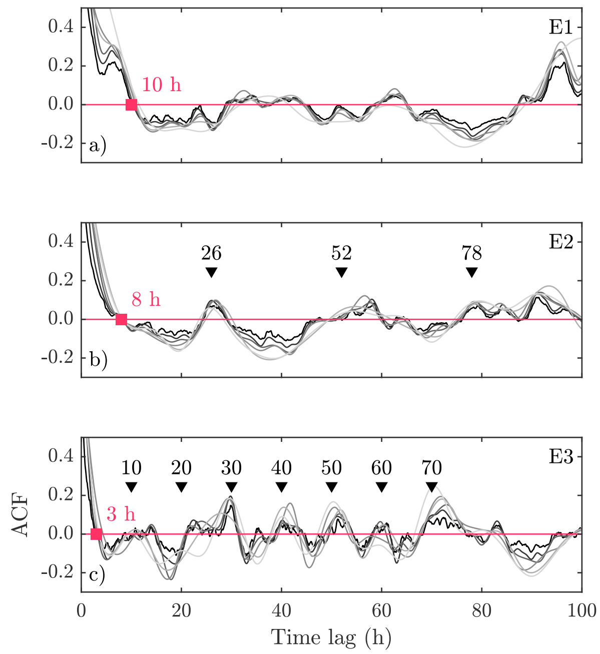

Figure 9. Autocorrelation function (ACF) of the bedload transport rates averaged over different sampling times for (a) experiment 1, (b) experiment 2, and (c) experiment 3. The black curves correspond to a 1-min sampling time. The grey curves correspond to sampling times within 1 h and 5 h (light shades stand for large sampling times).

in the longitudinal direction and are about 15–20 cm wide and 4–6 m long. The average deposition rates in these zones are approximately two to three times larger than in the central area of the flume. The range of values observed is respectively 2.2–10.4, 4.3–11.0, and 3.6–16.0 mm/h in experiment 1, 2, and 3. The arrangement of the main deposition zones is similar in each experiment: one on the right side and two (only one in experiment 1) on the left side. They are distributed along the whole flume length except in the most upstream part. Near the flume inlet, it appears that the center of the channel also undergoes intense sediment erosion/deposition during the experiments. This observation indicates that the sediment fed in the flume is first deposited in the bed before being transported further downstream.

The change in sediment supply magnitude between the experiments impacts the characteristics of the deposition zones appearing in Figure 10. As the sediment feed rate increases from 2.5 to 5.0 g/s between experiment 1 and 2, a third intense deposition zone appears on the left side of the upstream part of the flume. In addition, the deposition zones gets narrower and more stretched longitudinally. The maximum average deposition rate remains however about 1.0 cm/h although sediment erosion/deposition is more uniformly distributed over space in experiment 2. This latter observation is the result of the longer duration of experiment 2 which allowed more varied bed configurations to persist. The spatial configuration of deposition zones in experiment 3 is very similar to the one in experiment 2. However, as the sediment feed rate increased by 1.5, so did the maximum erosion rate which increased to about 1.5 cm/h. Sediment erosion and deposition processes therefore gained in intensity with increasing sediment feed rate. The comparison of the average deposition rates in Figure 10 with the topographical data revealed a clear correspondence between the spatial distribution of sediment erosion and deposition processes and the bar-and-pool morphology in the bed (Figure 2): intense erosion/deposition zones match the most common pool locations. The average deposition rates therefore reflect the morphological print of bedload transport and indicates that the pools store and release large amounts of sediment during the experiments. The bar-and-pool system plays a key role in the transport of sediment, the pools being the active part where it is channeled.

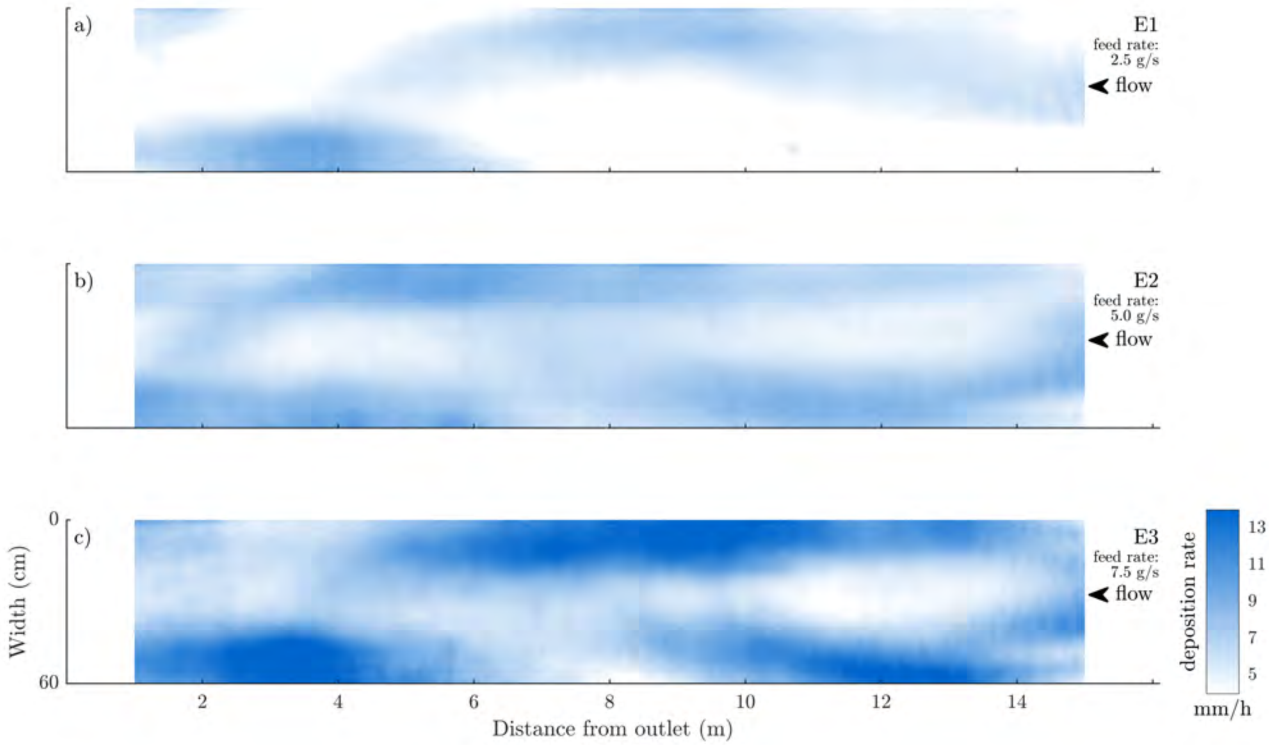

Figure 10. Spatial distribution of the average sediment deposition rates in the bed during (a) experiment 1, (b) experiment 2, and (c) experiment 3. The flume is viewed from the top and the flow direction is from right to left. Dark areas represent zones of intense sediment deposition.

The central part of the bed near the flume inlet underwent an intense sediment erosion/deposition activity during the experiments (Figure 10). The time series of the bed elevation in this area exhibited important fluctuations up to 10 cm and characterized by standard deviations of respectively 1.4, 1.8, and 0.8 cm in experiment 1, 2, and 3. A number of important degradation events in the most upstream part of the flume were observed to match intense bedload pulses at the flume outlet suggesting correlation at long timescales. The power spectra of the bedload transport rates and the bed elevation near the flume inlet are plotted in Figure 11 (for comparison purposes, the bedload transport rates were averaged over 10 min time steps). In each experiment, the spectrum of the transport rates and bed elevation saturates in the same low frequency range. In addition, several high energy peaks can be identified at the same frequencies in both spectrum. This similarity means that the maximum fluctuation timescale is the same for both time series and support the observation above that large-scale bedload transport rate fluctuations are correlated to bed elevation variations in the most upstream part of the flume. The entire length of the bed, covering several bar wave lengths, can therefore participate in generation of large-scale bedload pulses.

The bedload pulses recorded at the flume outlet represent sediment amounts substantially larger than what is supplied at the flume inlet during the same time periods. The erosion of bed material that, therefore, necessarily occurs leaves a print in the bed which shows that bed aggradation and degradation processes are localized in space (Figure 10). Moreover, at long timescales, we observed that the entire length of the

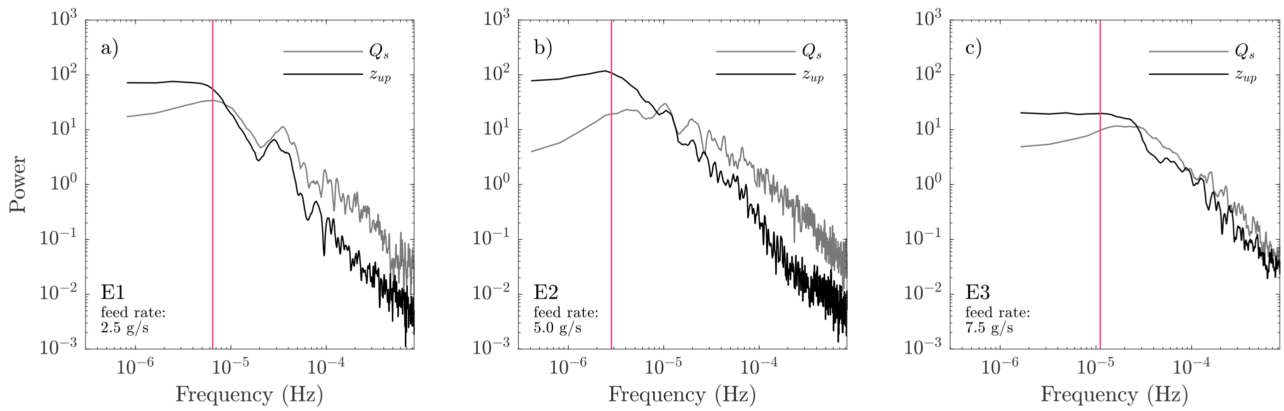

Figure 11. Power spectra of the bedload transport rates (Q_s) and of the bed elevation near the flume intlet (z_{up}) for (a) experiment 1, (b) experiment 2, and (c) experiment 3.

flume can contribute to bedload pulses (Figure 11). Hereafter, the longitudinal distribution of bedload transport during bedload pulses is further investigated by defining the *active length* as the downstream part of the bed of which overall erosion matches the amount of sediment evacuated at the flume outlet. It is computed by: (1) aggregating bed elevation measurements in the cross-sectional direction; (2) computing the change in bed mass since the last measurement at each cross section and for each measurement; and (3) integrating the change in bed mass along the flume length, starting from the outlet, until it matches the amount of sediment removed from the flume during the same time period. The active length is thus indicative of the bed part that delivers the sediment transported during bedload pulses under the hypothesis that between each bed scan the sediment mobilized in the bed is not deposited. In order to focus on intense bedload transport events, the active length was computed only when the mass evacuated was larger than the mass fed by 1.5 times. Note that the change in bed mass near the flume outlet ($x = 0$–1 m), where measurements are not available, was estimated based on the measurements at $x = 1$ m.

The histograms of the bed active length during bedload pulses shows a number preferential values (Figure 12). In experiment 1 and 2, three values multiple of 4 m appear clearly: 4, 8, and 12 m. By examining the corresponding bed topography measurements, these active length values were found to match the position of three bars and their adjacent pools (bar-pool pairs). Note that the theoretical bar length according to Yalin (1992) is about 6 times the flume width (i.e., 3.6 m) which is in agreement with the observations above. In experiment 2, which is the longest one (~560 h), bedload pulses have a tendency to originate from the most downstream bar-pool pair whereas in experiment 1 the contribution of each bar-pool pair is comparable. In experiment 3, the preferential values of the active length are less uniformly spaced. We explain this difference by the larger variability in bar characteristics (number, location, and shape) observed during this experiment. However, in all three experiments, the active length seems to be a function of the number of bar-pool pairs involved in sediment mobilization. The active length during low transport phases (i.e., when the mass evacuated is lower than the mass fed) were also computed and it appeared that the most frequent values were within 4 m of the flume outlet: when the bed undergoes overall aggradation, low bedload pulses are generally generated by erosion in the most downstream bar-pool pair. The fate of the sediment fed in the flume was also investigated using the same method: the change in bed mass was integrated starting from the flume inlet until it met the amount of sediment fed since the last bed scan. It appeared that the sediment supplied to the flume is preferentially deposited within the first meter of the inlet ($x = 15$–16 m) which supports previous results. These results indicate that the transport of sediment from the upstream part of the flume where it is fed to the downstream part is discontinuous and controlled by the bar-and-pool system. The sediment fed is first deposited close to the flume inlet, increasing the bed total volume asymmetrically, before being transported further downstream. The bed is therefore constantly disturbed in its upstream part and only a number of spatially delimited zones participate in the transport of sediment.

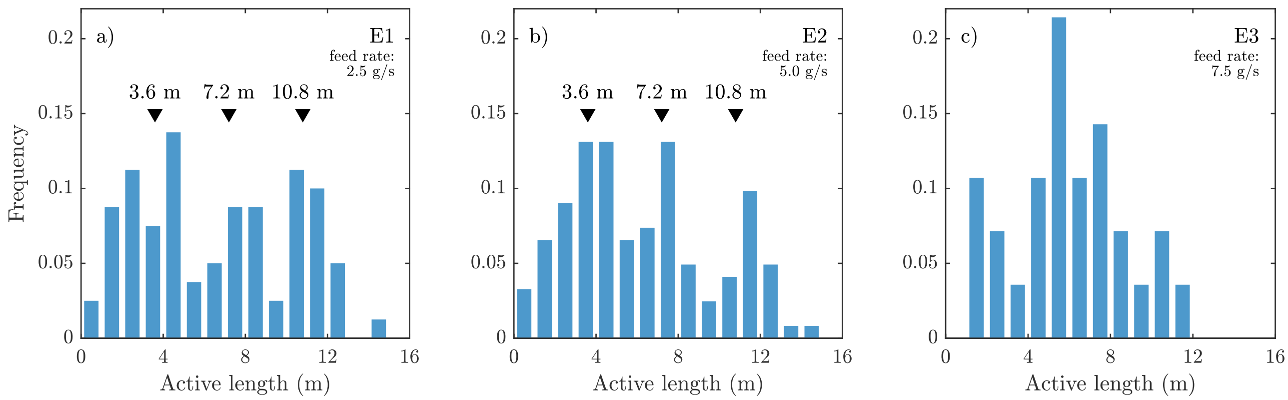

Figure 12. Distribution of the bed active length measured from the flume outlet during intense bedload transport events for (a) experiment 1, (b) experiment 2, and (c) experiment 3. The downward-pointing triangles indicate the theoretical position of bars.

Discussion

Bedload pulses

For each experiment, bedload transport exhibited a pulsating behavior marking the alternation between phases of low and intense transport. At the flume outlet, the transport rate varied around the mean value with fluctuations that could be 10 times higher than this mean value. This is consistent with other experimental studies carried out under steady flow conditions (Hubbell, 1987; Iseya and Ikeda, 1987; Kuhnle and Southard, 1988; Gomez et al., 1989; Hoey, 1992; Ancey et al., 2008; Recking et al., 2009; Singh et al., 2009; Ghilardi et al., 2014a; Ancey et al., 2015). As a consequence, the average bedload transport rate value does not reflect the most frequent state of the system although it is imposed by the boundary conditions.

In our experiments, bedload pulses were defined by their duration in addition to their frequency and magnitude. The inter-arrival times (related to both pulse duration and frequency) varied from minutes to hours: bedload pulses occurred intermittently. According to authors like Singh et al. (2009), this intermittency arises from the very nature of bedload transport at the particle scale, dominated by randomness. A contrasting view emerges from the analysis of the autocorrelation, which brings out a period behavior, in line with earlier observations (Cudden and Hoey, 2003; Ghilardi et al., 2014b). The dual behavior (a purely stochastic or deterministic and periodic process) might imply that bedload pulses are not only random realizations of stochastic processes, but also originate from deterministic mechanisms at play along the bed (Cudden and Hoey, 2003). In our experiments, periodicity was associated with timescales longer than ten hours, which corresponded approximately to the occurrence period of the largest bedload pulses. Moreover, these periods were also found to feature global changes in the bed volume. Such a regular sequence of sediment shortage and abundance suggests the existence of a maximum storage capacity of the bed. For a given bed configuration, this capacity dictates the frequency at which large-scale fluctuations occur. At higher frequencies (corresponding to periods of a few hours), periodicity in the bedload transport rate fluctuations was also observed using Fourier analysis (see in Dhont, 2017). This finding is consistent with what other authors obtained when relating the periodic character of bedload pulses to migrating bedforms (Kuhnle and Southard, 1988; Gomez et al., 1989; Ashmore, 1991; Hoey, 1992; Ghilardi et al., 2014b). These bed structures (see overview in Kuhnle, 1996) were also observed to cause bedload pulses in our experiments (Dhont and Ancey, 2018).

The fluctuations in the transport rates were described for each experiment based on the intensity and intermittency of bedload pulses. Three fluctuation regimes arose from the results obtained, each associated with one of the sediment feed rate tested. It appears that bedload pulses tended to be shorter, more frequent and of lower magnitude as the feed rate increased. Note that the global hydraulic conditions varied from one experiment to another because of the changes observed in the bed morphology: the average stream was larger in experiments with larger sediment feed rates. These tendencies are consistent with the findings of other authors who described in general "smoother" bedload transport rate time series (i.e., less bursty) at higher flow rates (Singh et al., 2009). For instance, Kuhnle and Southard (1988) have observed fluctuations of lower magnitude when the sediment feed rate in their experiments with poorly-sorted gravel increases. More generally, Ghilardi et al. (2014b), who have tested various combinations of water discharges and sediment feed rates in a gravel-bed flume with large boulders, have reported that the magnitude, period and duration of the pulses decrease when the stream power is increased. In our study, this effect was quantified based on how the relationships between pulse characteristics (duration, frequency, and magnitude) were affected by the different sediment feed rate tested.

Mass balance and bed equilibrium

In flume investigations carried out under controlled feeding conditions, the time-averaged transport rate matches the imposed sediment feed rate since the experimental procedures are devised to ensure a bed equilibrium driven by mass balance or *dynamic equilibrium* according to the terminology used by a number of authors (Recking et al., 2009)—that usage is, however, not consensual (Thorn and Welford, 1994). To achieve these conditions, the common method is to wait until the time-averaged bedload transport rate reaches the average sediment feed rate before starting the measurement campaign (Singh et al., 2009). In this study, we addressed this issue by introducing the *convergence time*, which is a measure of the shortest observation time necessary to guarantee overall bed equilibrium in the system regardless of the details (that is, the fluctuations of the bed surface). The convergence time can thus be seen as the time necessary to capture all fluctuations types in the system, including the largest ones. In addition, the convergence time indicates how bedload pulses and low transport phases, respectively, affect the average bedload transport rate. In our experiments, low transport phases are the limiting factor slowing the achievement of dynamic bed equilibrium. This observation highlights the part played by low transport phases even though little sediment is carried during these phases: what matters here is not transport, but sediment storage. The more sediment accumulates in the pools, the larger and longer the bedload pulses. The convergence time is a useful albeit indirect measure of the store-and-release mechanism that punctuates bed evolution.

Bed response

The changes to bed topography between the experiments characterized by different sediment feed rates reflect the effect of increased sediment supply conditions on the alternate bar configuration, a topic that has drawn much attention (Lisle et al., 1997; Cui et al., 2003; Madej et al., 2009; Pryor et al., 2011; Podolak and Wilcock, 2013; Mueller and Pitlick, 2014; Zunka et al., 2015; Elgueta-Astaburuaga and Hassan, 2017). In each experiment, the evolution of the bed from a flat configuration to an alternate bar configuration resulted in an increased transport capacity. This is consistent with the conclusion of Francalanci et al. (2012), who investigated the effect of similar bedforms on flow resistance. We also observed that the general bed response to an increase in sediment supply was an increase in the average slope and a more braided configuration, as reported in other studies (Madej et al., 2009; Pryor et al., 2011; Mueller and Pitlick, 2014). These changes in the bed geometry both contribute to increasing the transport capacity and accommodating to the feed rate (Podolak and Wilcock, 2013). However, the increase in average bed slope between experiment 1 and 3 was vanishingly small although the sediment feed rate was doubled. The increase in transport capacity was therefore mainly due to the changes to the alternate bar configuration (increased braiding), which illustrates the finding of several authors that adjustment in bar spatial configuration can increase locally the bed shear stress without necessarily changing its mean value (Paola, 1996; Nicholas, 2000; Ferguson, 2003; Francalanci et al., 2012; Podolak and Wilcock, 2013; Mueller and Pitlick, 2014). Our experiments suggests that the transport capacity is affected by the storage of sediment in the bed. We concur with Lisle and Church (2002) and Madej et al. (2009) that better understanding sediment transport-storage relationships in gravel-bed rivers is the key to explaining their morphodynamics.

Conclusion

This study examined how decreasing sediment supply impacts bedload transport and bed topography (here, alternate bars and pools) in a gravel-bed flume. Special emphasis was given to determining the different timescales of the physical processes at play. Three long-duration experiments were conducted under steady flow and sediment feeding conditions, each with a different sediment feed rate.

As described in other studies (Podolak and Wilcock, 2013), we observed that the change in sediment supply primarily affected bed morphology: the channel adjusted its transport capacity by increasing the mean slope and evolving toward a more braided configuration. The response of the bed slope was, however, not linear by contrast with what Lane's balance states (Lane, 1955). This suggests that local changes to the bed geometry contributed to increasing the bed shear stress. Decreasing sediment supply changed autogenic fluctuations of bedload transport rates: bedload pulses were larger in magnitude, lasted longer, and occurred less frequently in experiments with low feed rates. Moreover, the quasi-periodic character of large-scale fluctuations was less obvious when decreasing the sediment feed rate. This suggests that under increased bedload transport conditions, the bed acted like a sediment buffer, with sediment trapped and stored in pools. As the buffer had a fixed storage capacity, the bed intermittently released finite volumes of sediment. This provided clear evidence that bed evolution was punctuated by this store-and-release mechanism.

Quantifying how the bed accommodated to sediment feed rates turned out to be difficult: (i) the bed response was nonlinear (as discussed above, doubling the feed rate did not lead to doubling the mean bed slope); (ii) the system fluctuated much (in terms of bed elevation and bedload transport rate) to the point that the mean values did not reflect the most frequent state of the system; (iii) these mean values (that is, mean slope and bedload transport rate) were forced by the boundary conditions; (iv) bedload pulses occurred intermittently, and were separated by phases of low transport intensity; (v) the timescales that emerged from the analysis of bedload transport rates varied nonlinearly with the strength of sediment transport; (vi) time-dependent processes involving slow storage and fast release phases drove bed evolution. Although we failed to make headway towards full quantification, our experimental set the stage for future research in this direction.

Our results also shed new light how changing sediment supply impacts sediment transport, and thus can help make river restoration strategies more efficient. They provide evidence that the shortage of sediment supply does not only affect bed morphology, but also the strength of fluctuations by increasing intermittency in bedload transport. This intermittent character arises from the buffer role played by the bed and the store-and-release mechanism. For bar-and-pool morphologies, this mechanism takes mainly place in pools. In an earlier publication, we showed how sediment waves migrating from pool to pool generated most bedload pulses, but not the largest ones (Dhont and Ancey, 2018). Indeed, largest pulses were caused by bar failures, which led to a global reworking of the bed. In light of this, we think that sediment replenishment is all the more efficient that the injections (location and strength) are compatible with the store-and-release mechanism at play in the reach. For a given bed morphology, depending on where and how it is introduced, sediment can either be flushed out or, on the contrary, be deposited, and thereby increase morphological variability.

Acknowledgments

The authors acknowledge the support of the Swiss National Science Foundation (grant 200021_129538).

References

Ancey, C., Bohorquez, P., and Heyman, J. (2015). "Stochastic interpretation of the advection-diffusion equation and its relevance to bed load transport." *Journal of Geophysical Research: Earth Surface*, 120(12), 2529–2551 2014JF003421.

Ancey, C., Davison, A. C., Boehm, T., Jodeau, M., and Frey, P. (2008). "Entrainment and motion of coarse particles in a shallow water stream down a steep slope." *Journal of Fluid Mechanics*, 595, 83–114.

Ashmore, P. (1991). "Channel morphology and bed load pulses in braided, gravel-bed streams." *Geografiska Annaler*, 73A(1), 37–52.

Battisacco, E., Franca, M. J., and Schleiss, A. J. (2016). "Sediment replenishment: Influence of the geometrical configuration on the morphological evolution of channel-bed." *Water Resources Research*, 52(11), 8879–8894.

Brandt, S. A. (2000). "Classification of geomorphological effects downstream of dams." *CATENA*, 40(4), 375–401.

Cudden, J. R. and Hoey, T. B. (2003). "The causes of bedload pulses in a gravel channel: the implications of bedload grain-size distributions." *Earth Surface Processes and Landforms*, 28(13), 1411–1428.

Cui, Y., Parker, G., Lisle, T. E., Gott, J., Hansler-Ball, M. E., Pizzuto, J. E., Allmendinger, N. E., and Reed, J. M. (2003). "Sediment pulses in mountain rivers: 1. Experiments." *Water Resources Research*, 39(9) 1239.

Dhont, B. (2017). "Sediment pulses in a gravel-bed flume with alternate bars." Ph.D. thesis, École Polytechnique Fédérale de Lausanne, Lausanne, Switzerland.

Dhont, B. and Ancey, C. (2018). "Are bedload transport pulses in gravel bed rivers created by bar migration or sediment waves?." *Geophysical Research Letters*, 45(11), 5501–5508.

Dhont, B., Rousseau, G., and Ancey, C. (2017). "Continuous monitoring of bed-load transport in a laboratory flume using an impact sensor." *Journal of Hydraulic Engineering*, 143(6), 04017005.

Elgueta-Astaburuaga, M. A. and Hassan, M. A. (2017). "Experiment on temporal variation of bed load transport in response to changes in sediment supply in streams." *Water Resources Research*, 53(1), 763–778.

Elgueta-Astaburuaga, M. A., Hassan, M. A., Saletti, M., and Clarke, G. K. C. (2018). "The effect of episodic sediment supply on bedload variability and sediment mobility." *Water Resources Research*, 54(9), 6319–6335.

Emmett, W. W. (1975). "The channels and waters of the upper Salmon River area, Idaho." *USGS Professional Paper*, 870A.

Ferguson, R. (2003). "The missing dimension: effects of lateral variation on 1-d calculations of fluvial bedload transport." *Geomorphology*, 56(1), 1–14.

Francalanci, S., Solari, L., Toffolon, M., and Parker, G. (2012). "Do alternate bars affect sediment transport and flow resistance in gravel-bed rivers?." *Earth Surface Processes and Landforms*, 37(8), 866–875.

Fryirs, K. (2013). "(dis)connectivity in catchment sediment cascades: a fresh look at the sediment delivery problem." *Earth Surface Processes and Landforms*, 38(1), 30–46.

Furbish, D. J., Schmeeckle, M. W., Schumer, R., and Fathel, S. L. (2016). "Probability distributions of bed load particle velocities, accelerations, hop distances, and travel times informed by jaynes's principle of maximum entropy." *Journal of Geophysical Research: Earth Surface*, 121(7), 1373–1390.

Ghilardi, T., Franca, M. J., and Schleiss, A. J. (2014a). "Bed load fluctuations in a steep channel." *Water Resources Research*, 50(8), 6557–6576.

Ghilardi, T., Franca, M. J., and Schleiss, A. J. (2014b). "Period and amplitude of bedload pulses in a macro-rough channel." *Geomorphology*, 221, 95–103.

Gomez, B. (1991). "Bedload transport." *Earth-Science Reviews*, 31(2), 89–132.

Gomez, B., Naff, R. L., and Hubbell, D. W. (1989). "Temporal variations in bedload transport rates associated with the migration of bedforms." *Earth Surface Processes and Landforms*, 14(2), 135–156.

Heyman, J., Mettra, F., Ma, H. B., and Ancey, C. (2013). "Statistics of bedload transport over steep slopes: Separation of time scales and collective motion." *Geophysical Research Letters*, 40(1), 128–133.

Hoey, T. B. (1992). "Temporal variations in bedload transport rates and sediment storage in gravel-bed rivers." *Progress in Physical Geography*, 16(3), 319–338.

Hoey, T. B. and Sutherland, A. J. (1991). "Channel morphology and bedload pulses in braided rivers: a laboratory study." *Earth Surface Processes and Landforms*, 16(5), 447–462.

Hoffman, D. F. and Gabet, E. J. (2007). "Effects of sediment pulses on channel morphology in a gravel-bed river." *Geological Society of America Bulletin*, 119(1-2), 116–125.

Hubbell, D. W. (1987). *Sediment Transport in Gravel-Bed Rivers*. John Wiley & Sons Ltd, Chichester, UK, Chapter Bed load sampling and analysis, 89–118.

Iseya, F. and Ikeda, H. (1987). "Pulsations in bedload transport rates induced by a longitudinal sediment sorting: A flume study using sand and gravel mixtures." *Geografiska Annaler*, 69A(1), 15–27.

James, L. A. (2010). "Secular sediment waves, channel bed waves, and legacy sediment." *Geography Compass*, 4(6), 576–598.

Jerolmack, D. J. and Paola, C. (2010). "Shredding of environmental signals by sediment transport." *Geophysical Research Letters*, 37(19) L19401.

Kantoush, S. A., T. S. T. S. and Murasaki, M. (2010). "Impacts of sediment flushing on channel evolution and morphological processes: Case study of the kurobe river, japan." *River Flow 2010*, A. Dittrich, K. Koll, J. Aberle, and P. Geisenhainer, eds., Bundesanstal für Wasserbau, Karlsruhe, 1165–1173, <https://henry.baw.de/handle/20.500.11970/99765>.

Kondolf, G. M. (1997). "Hungry water: Effects of dams and gravel mining on river channels." *Environmental Management*, 21(4), 533–551.

Kuhnle, R. A. (1996). *Advances in fluvial dynamics and stratigraphy*. John Wiley & Sons Ltd, Chichester, UK, Chapter Unsteady transport of sand and gravel mixtures, 183–201.

Kuhnle, R. A. and Southard, J. B. (1988). "Bed load transport fluctuations in a gravel bed laboratory channel." *Water Resources Research*, 24(2), 247–260.

Lane, E. W. (1955). "The importance of fluvial morphology in hydraulic engineering." *Proceedings of the American Society of Civil Engineers*, 81(745), 1–17.

Lanzoni, S. (2000). "Experiments on bar formation in a straight flume: 2. Graded sediment." *Water Resources Research*, 36(11), 3351–3363.

Lisle, T. E. and Church, M. (2002). "Sediment transport-storage relations for degrading, gravel bed channels." *Water Resources Research*, 38(11) 1219.

Lisle, T. E., Iseya, F., and Ikeda, H. (1993). "Response of a channel with alternate bars to a decrease in supply of mixed-size bed load: A flume experiment." *Water Resources Research*, 29(11), 3623–3629.

Lisle, T. E., Nelson, J. M., Pitlick, J., Madej, M. A., and Barkett, B. L. (2000). "Variability of bed mobility in natural, gravel-bed channels and adjustments to sediment load at local and reach scales." *Water Resources Research*, 36(12), 3743–3755.

Lisle, T. E., Pizzuto, J. E., Ikeda, H., Iseya, F., and Kodama, Y. (1997). "Evolution of a sediment wave in an experimental channel." *Water Resources Research*, 33(8), 1971–1981.

Ma, H., Heyman, J., Fu, X., Mettra, F., Ancey, C., and Parker, G. (2014). "Bed load transport over a broad range of timescales: Determination of three regimes of fluctuations." *Journal of Geophysical Research: Earth Surface*, 119(12), 2653–2673 2014JF003308.

Madej, M. A., Sutherland, D. G., Lisle, T. E., and Pryor, B. (2009). "Channel responses to varying sediment input: A flume experiment modeled after Redwood Creek, California." *Geomorphology*, 103(4), 507–519.

Mettra, F. (2014). "Morphodynamic mechanisms in steep channels: from local processes to large-scale evolution." Ph.D. thesis, École Polytechnique Fédérale de Lausanne, Lausanne, Switzerland.

Miwa, H. and Daido, A. (1995). "Fluctuations in bed-load transport rate in channel with alternate bars." *In: Management of Sediment: Philosophy, Aims, and Techniques. Proceedings of the Sixth International Symposium on River Sedimentation, New Delhi, India*, Oxford & IBH publishing, 641–648.

Mueller, E. R. and Pitlick, J. (2014). "Sediment supply and channel morphology in mountain river systems: 2. Single thread to braided transitions." *Journal of Geophysical Research: Earth Surface*, 119(7), 1516–1541 2013JF003045.

Nelson, P. A., Venditti, J. G., Dietrich, W. E., Kirchner, J. W., Ikeda, H., Iseya, F., and Sklar, L. S. (2009). "Response of bed surface patchiness to reductions in sediment supply." *Journal of Geophysical Research: Earth Surface*, 114(F2).

Nicholas, A. (2000). "Modelling bedload yield in braided gravel bed rivers." *Geomorphology*, 36(1), 89–106.

Paola, C. (1996). *Coherent Flow structures in Open Channels*. John Wiley & Sons Ltd, Chichester, UK, Chapter Incoherent structure: Turbulence as a metaphor for stream braiding, 705–723.

Podolak, C. J. P. and Wilcock, P. R. (2013). "Experimental study of the response of a gravel streambed to increased sediment supply." *Earth Surface Processes and Landforms*, 38(14), 1748–1764.

Pryor, B. S., Lisle, T. E., Montoya, D. S., and Hilton, S. (2011). "Transport and storage of bed material in a gravel-bed channel during episodes of aggradation and degradation: A field and flume study." *Earth Surface Processes and Landforms*, 36(15), 2028–2041.

Radice, A. (2009). "Use of the Lorenz curve to quantify statistical nonuniformity of sediment transport rate." *Journal of Hydraulic Engineering*, 135(4), 320–326.

Recking, A., Frey, P., Paquier, A., and Belleudy, P. (2009). "An experimental investigation of mechanisms involved in bed load sheet production and migration." *Journal of Geophysical Research: Earth Surface*, 114 F03010.

Reid, I., Frostick, L. E., and Layman, J. T. (1985). "The incidence and nature of bedload transport during flood flows in coarse-grained alluvial channels." *Earth Surface Processes and Landforms*, 10(1), 33–44.

Rickenmann, D., Turowski, J. M., Fritschi, B., Wyss, C., Laronne, J. B., Barzilai, R., Reid, I., Kreisler, A., Aigner, J., Seitz, H., and Habersack, H. (2014). "Bedload transport measurements with impact plate geophones: comparison of sensor calibration in different gravel-bed streams." *Earth Surface Processes and Landforms*, 39(7), 928–942.

Roseberry, J. C., Schmeeckle, M. W., and Furbish, D. J. (2012). "A probabilistic description of the bed load sediment flux: 2. particle activity and motions." *Journal of Geophysical Research: Earth Surface*, 117(F3).

Saletti, M., Molnar, P., Zimmermann, A., Hassan, M. A., and Church, M. (2015). "Temporal variability and memory in sediment transport in an experimental step-pool channel." *Water Resources Research*, 51(11), 9325–9337.

Singh, A., Fienberg, K., Jerolmack, D. J., Marr, J. D. G., and Foufoula-Georgiou, E. (2009). "Experimental evidence for statistical scaling and intermittency in sediment transport rates." *Journal of Geophysical Research: Earth Surface*, 114(F1) F01025.

Sklar, L. S., Fadde, J., Venditti, J. G., Nelson, P., Wydzga, M. A., Cui, Y., and Dietrich, W. E. (2009). "Translation and dispersion of sediment pulses in flume experiments simulating gravel augmentation below dams." *Water Resources Research*, 45(8).

Thorn, C. E. and Welford, M. R. (1994). “The equilibrium concept in geomorphology.” *Annals of the Association of American Geographers*, 84(4), 666–696.

Venditti, J. G., Nelson, P. A., Minear, J. T., Wooster, J., and Dietrich, W. E. (2012). “Alternate bar response to sediment supply termination.” *Journal of Geophysical Research: Earth Surface*, 117(F2) F02039.

Whiting, P. J., Dietrich, W. E., Leopold, L. B., Drake, T. G., and Shreve, R. L. (1988). “Bedload sheets in heterogeneous sediment.” *Geology*, 16(2), 105.

Wohl, E. (2018). *Sustaining River Ecosystems and Water Resources*. Springer International Publishing, Cham, Chapter Toward Sustainable Rivers and Water Resources, 105–141.

Yalin, M. S. (1972). *Mechanics of Sediment Transport*. Pergamon Press Ltd, Oxford, UK.

Yalin, M. S. (1992). *River Mechanics*. Pergamon Press Ltd, Oxford, UK.

Zunka, J. P. P., Tullos, D. D., and Lancaster, S. T. (2015). “Effects of sediment pulses on bed relief in bar-pool channels.” *Earth Surface Processes and Landforms*, 40(8), 1017–1028.